GUST AND DOWNWARD MOMENTUM TRANSPORT IN THE ATMOSPHERIC SURFACE LAYER

TAIICHI HAYASHI

Shionomisaki Wind Effect Laboratory, Disaster Prevention Research Institute, Kyoto University, Wakayama, Japan

(Received in final form 11 June, 1991)

Abstract. The intermittent structure of the turbulent wind field in the atmospheric surface layer is investigated by conditional sampling methods. The results show that downward momentum can be transported efficiently during a peak gust. The horizontal structure of the gust is also revealed by observing the spatial structure of wind speed fluctuations from a network of 28 anemometers. The high wind region consists of a gust front with a sudden increase of wind speed at the front and a slow decrease to its rear. The development of the gust front is related closely to the momentum flux during the short time of passage of the gust.

1. Introduction

The wind near the ground is unsteady and inhomogeneous in time and space. This may be seen by the bending motion of grass in response to wind gusts, which Inoue (1955) called the honami (ear-wave), in the case of a rice paddy. Strong winds are also gusty, and spatial distributions of raindrops in a storm are also not uniform; dense and thin rain shadows, which are produced by divergence or convergence of surface winds, can usually be seen. The sudden increase of surface wind speed is like a front moving with the wind, as was first pointed out by Sherlock (1952), who introduced the term *gust front*.

However, wind fluctuations near the ground have been treated as stochastic for a long time and their statistical properties have been analysed, postulating steady state, in terms of parameters such as mean, variance and power spectral density. These statistical analyses obscure the intermittent nature of wind fluctuations.

The organized motions have been identified from flow visualization techniques in laboratory turbulent flows (Kline *et al.*, 1967; Grass, 1971; Chen and Blackwelder, 1978; Antonia *et al.*, 1979). Many conditional sampling methods have been developed to identify organized structures and some have succeeded in explaining the laboratory experiments. One such method is quadrant analysis (Willmarth and Lu, 1972; Wallace *et al.*, 1972; Nakagawa and Nezu, 1977) and another is the VITA (Variable Interval Time Average) method (Blackwelder and Kaplan, 1976; Schols, 1985). In the atmospheric surface layer, however, observational data on the intermittency of the transport of momentum and scalars are still sparse.

In the present paper, the spatial structure of a gust front in high wind condition is studied, using a network of 28 anemometers. And downward momentum trans-

Boundary-Layer Meteorology **58**: 33–49, 1992.

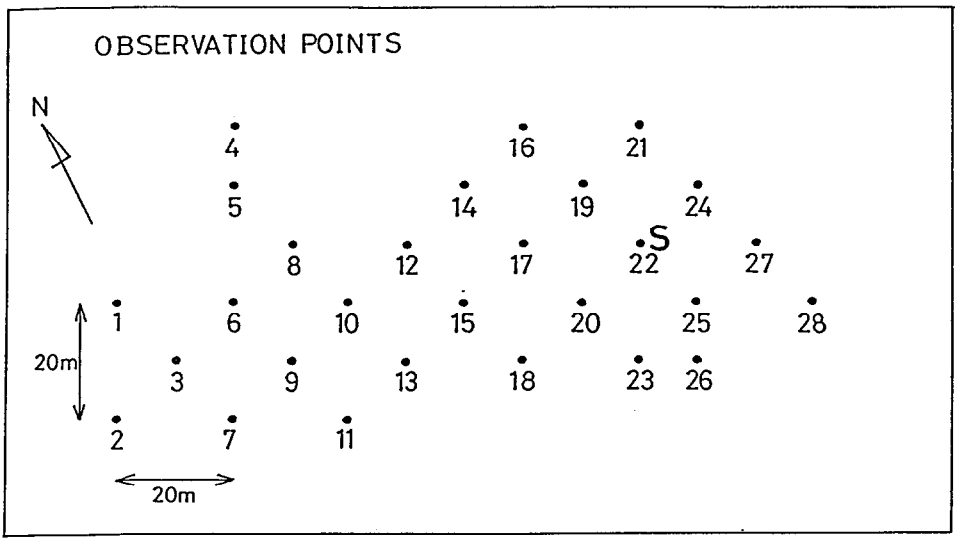

Fig. 1. The arrangement of cup anemometers and a sonic anemometer in the observation network. The numbers show the locations of cup anemometers and "*S*" shows the location of the sonic anemometer.

port at the gust, observed by a sonic anemometer, is analysed using a simple conditional sampling method. The relation between the gust front and downward momentum transport is also investigated.

2. Observations

Observations of the structure of storm gusts were carried out at the test field of the Shionomisaki Wind Effect Laboratory, Kyoto University in the winter of 1980 to 1981. Turbulent fluctuations of the wind velocity components were measured by a three-dimensional sonic anemometer (Kaijo Denki, PAT 311-1, Mitsuta, 1974), which was installed at a height of 12 m on a 16.5 m tall tower. Around the sonic anemometer, 28 cup anemometers were set up on top of 8.25 m towers. These towers were arranged to make a two-dimensionally uniform network. The arrangement of cup anemometers and of the sonic anemometer is shown in Figure 1. The signals from the sonic anemometer were sampled at 4 Hz and recorded on magnetic tape, together with the signals obtained from the cup anemometers. Details of measurement and two-dimensional space correlation properties have been reported in a previous paper (Hayashi, 1991).

3. Statistics of Wind Fluctuations

Statistical properties such as mean, rms, skewness and flatness of the three components of wind velocity fluctuations, u, v and w measured by the sonic anemometer

TABLE I

Statistics of three components of wind velocity, u, v and w in twelve observational runs

Run	Mean	RMS			Skewness			Flatness		
	$m\,s^{-1}$	σ_u $m\,s^{-1}$	σ_v $m\,s^{-1}$	σ_w $m\,s^{-1}$	S_u	S_v	S_w	F_u	F_v	F_w
1	14.30	3.38	2.68	2.03	0.14	0.14	0.11	2.82	3.55	3.20
2	13.62	3.50	2.41	1.89	0.28	−0.02	0.09	2.90	3.19	3.15
3	12.21	2.88	2.42	1.72	0.11	−0.35	0.09	2.90	3.33	3.10
4	11.21	3.63	2.49	1.85	0.50	0.12	0.02	3.22	3.11	3.26
5	9.12	2.70	1.92	1.45	0.30	0.12	0.08	2.89	3.69	3.26
6	7.54	2.31	1.92	1.29	0.23	−0.06	0.12	3.16	3.25	3.09
7	8.20	2.27	2.03	1.32	0.17	−0.08	0.24	2.75	3.02	3.26
8	10.20	2.56	2.13	1.61	0.10	−0.08	0.09	2.80	3.41	3.54
9	9.71	2.54	2.15	1.53	0.00	−0.15	0.17	2.61	3.09	3.35
10	10.76	3.19	2.44	1.74	0.25	−0.20	0.15	2.92	3.17	3.09
11	7.53	2.29	1.77	1.22	0.43	−0.28	0.19	3.48	3.36	3.43
12	6.90	1.95	1.66	1.23	−0.04	−0.21	0.04	2.82	3.22	3.13

are shown in Table I. The mean wind is in the range of $6.90\,m\,s^{-1}$ to $14.03\,m\,s^{-1}$, and atmospheric stratification was assumed to be near the neutral condition. The distribution of the joint probability density of u and w for Run 1 is shown in Figure 2; u and w are scaled by the rms values σ_u and σ_w. The horizontal component u extends from $-2.5\sigma_u$ to $3.5\sigma_u$ and the vertical component w from $-4.5\sigma_w$ to $4.5\sigma_w$. The deviation of this probability density distribution from the two-dimensional Gaussian distribution $P(u_n, w_n)$ is shown in Figure 3.

$$P(u_n, w_n)=(1/2\pi(1-r^2)^{1/2})\exp(-(u_n^2+2ru_nw_n+w_n^2))/2(1-r^2)) \tag{1}$$

where $u_n = u/\sigma_u$, $w_n = w/\sigma_w$ and $r = uw/\sigma_u\sigma_w$. In the case of Run 1, $\sigma_u = 3.38\,m\,s^{-1}$, $\sigma_w = 2.03\,m\,s^{-1}$ and $uw = -2.15\,m^2\,s^{-2}$. The distribution obeys the Gaussian distribution fairly well in the range $\pm 2\sigma$ or so but it deviates from the Gaussian distribution whenever deviations of u and w are large.

The statistics of vertical momentum transport uw are shown in Table II. The skewness is negative for all runs and -1.35 on the average. The flatness is 11.35 on average and has a sharp peak at the origin compared with the Gaussian distribution. The example of the probability density distribution for Run 1 is plotted in Figure 4. In the regions far from the origin, where $uw/\sigma_{uw} < -2$ and $3 < uw/\sigma_{uw}$, the observed probability density exceeds the Gaussian probability density given by the solid line.

4. Quadrant Representation of Momentum Flux

The instantaneous vertical transport of momentum $-uw$, is sorted into quadrants, according to the sign of the two wind fluctuating components, u and w (Willmarth

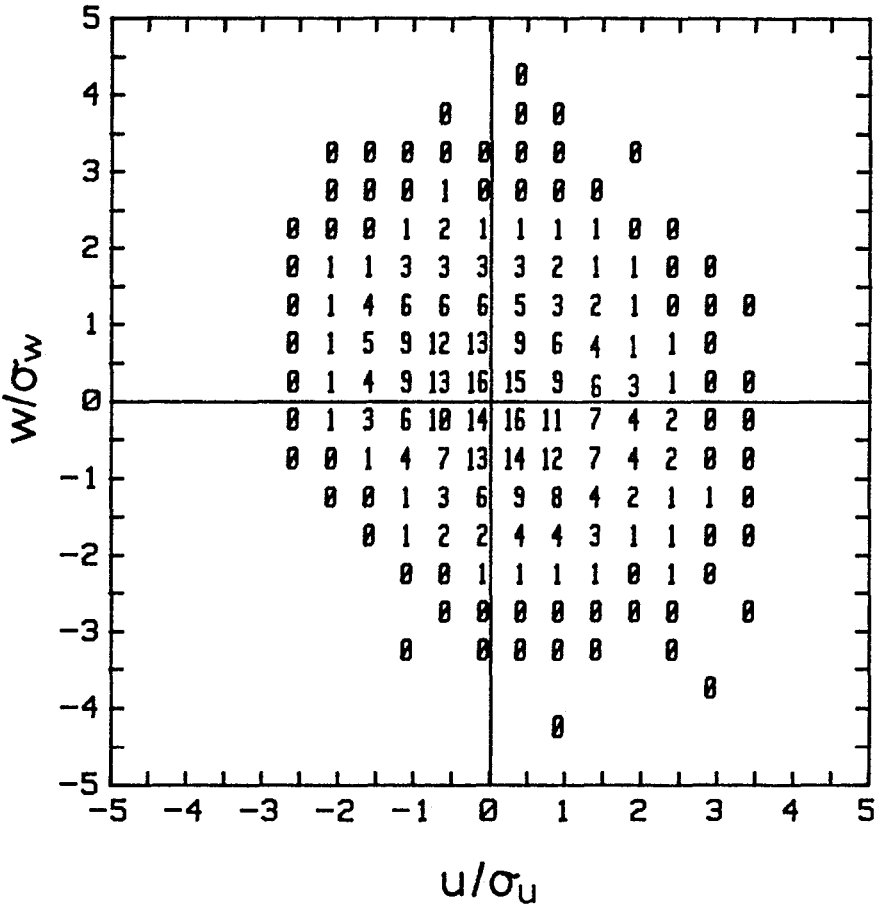

Fig. 2. Joint probability density (%) between longitudinal and vertical wind velocity fluctuations, u and w, u and w are normalized by their rms values respectively.

and Lu, 1972). The conditional sampling method was developed for the quantitative analysis of vertical momentum transport associated with burst phenomena in laboratory experiments (Willmarth and Lu, 1972; Lu and Willmarth, 1973; Nakagawa and Nezu, 1977). The method has also been applied to studies of intermittent transport processes over a plant canopy (Finnigan, 1979; Raupach, 1981; Shaw *et al.*, 1983; Gao *et al.*, 1989).

Quadrants are divided by the u and w axes, as follows,

$i = 1;$	$u > 0$ and $w > 0,$	outward interaction
$i = 2;$	$u < 0$ and $w > 0,$	ejection
$i = 3;$	$u < 0$ and $w < 0,$	inward interaction
$i = 4;$	$u > 0$ and $w < 0,$	sweep.

Quadrants 2 and 4 contribute to downward momentum transport, while quadrants

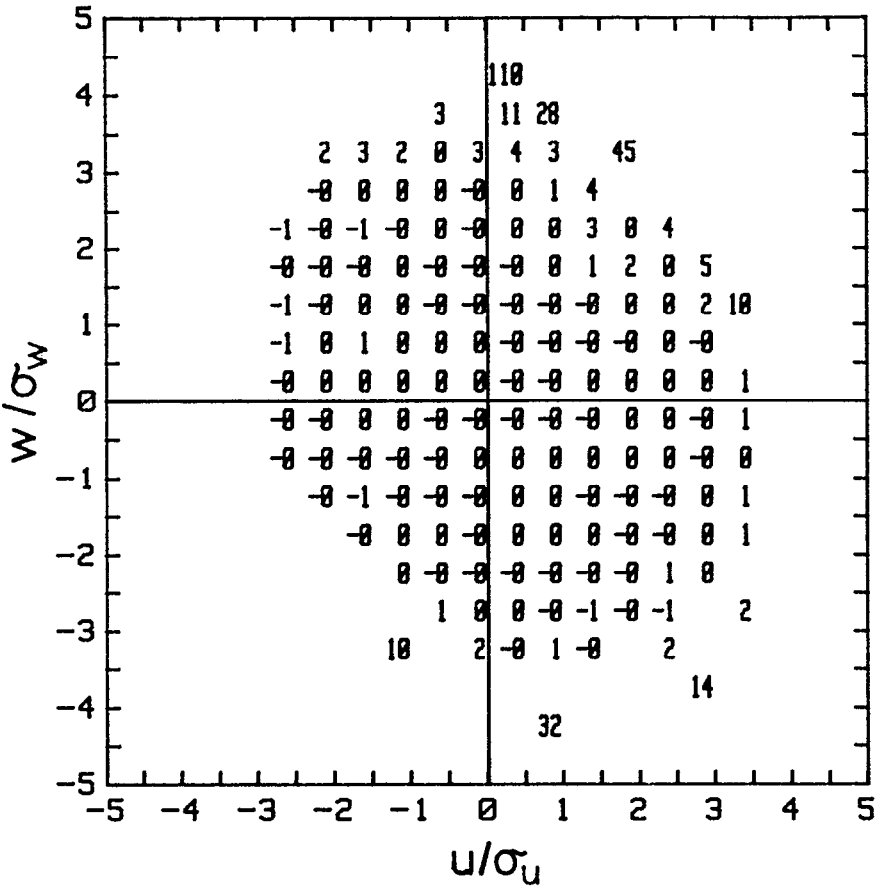

Fig. 3. Relative difference (%) of the joint probability density between u and w show in Figure 2 and the Gaussian distribution.

1 and 3 are responsible for upward fluxes. Around the origin of the uw plane, a hyperbolic hole is defined as the fifth region, as follows,

$$|uw| \leqq H \cdot |\overline{uw}| , \tag{2}$$

where H is called the hole size and the bar indicates a time average.

The conditional average of vertical momentum flux $\langle uw \rangle_{i,H}$ in the ith quadrant and outside of hole size H can be written as,

$$\langle uw \rangle_{i,H} = \lim_{T \to \infty} 1/T \int_0^{\infty} u(t) w(t) I_{i,H}(u(t), w(t))\, \mathrm{d}t \tag{3}$$

where $I_{i,H}(u(t), w(t))$ is the indicator function defined by,

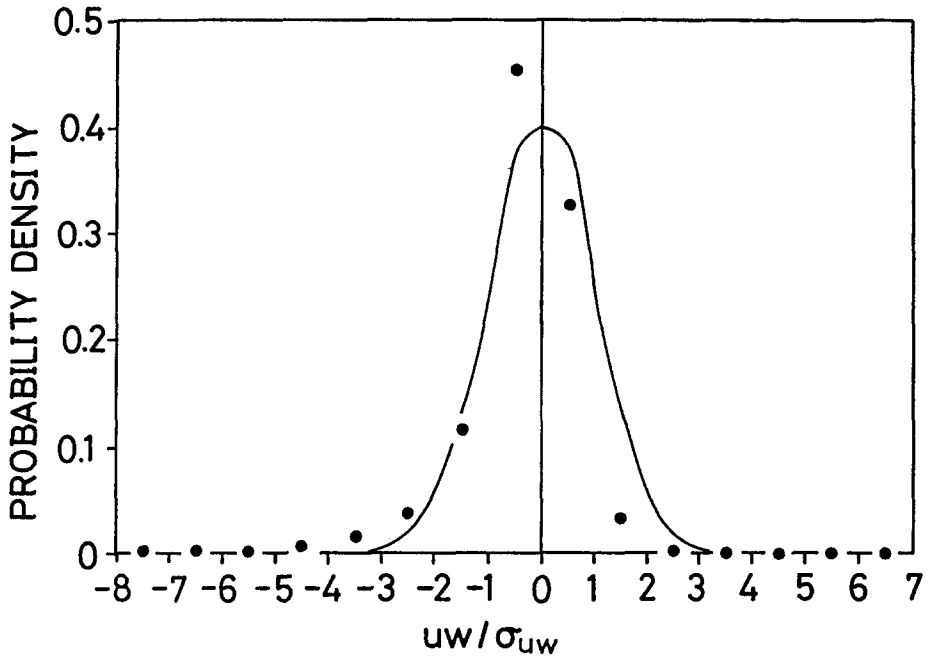

Fig. 4. Probability density of vertical momentum flux uw. uw is normalized by rms value of uw. Solid line shows the Gaussian distribution.

TABLE II

Statistics of vertical transport of momentum uw

Run	Mean $-uw$ $m^2 s^{-2}$	RMS σ_{uw} $m^2 s^{-2}$	Skewness S_{uw}	Flatness F_{uw}	Upward maximum $m^2 s^{-2}$	Downward maximum $m^2 s^{-2}$
1	2.15	6.95	−1.43	11.20	−34.75	72.79
2	2.32	6.70	−1.16	8.87	−41.43	51.15
3	1.75	4.97	−1.37	10.26	−27.02	49.06
4	2.26	6.74	−1.65	15.46	−38.01	88.50
5	1.41	3.78	−0.97	9.31	−33.04	36.12
6	0.95	3.23	−1.33	10.87	−27.96	33.01
7	1.03	3.09	−1.36	8.79	−15.36	23.03
8	1.20	4.18	−1.05	9.14	−24.79	32.45
9	1.39	3.87	−0.83	9.43	−39.10	27.44
10	2.23	5.60	−1.58	12.26	−13.51	66.53
11	0.98	3.05	−2.09	22.01	−28.85	43.15
12	0.86	2.40	−1.32	9.58	−10.96	22.05

$$I_{i,H}(u(t), w(t)) = \begin{cases} 1, & \text{if the point } (u, w) \text{ is in the } i\text{th quadrant and outside of the hole and } |uw| > H \cdot |\overline{uw}|, \\ 0, & \text{if the point is inside the hole and } |uw| \leqq H \cdot |\overline{uw}|. \end{cases}$$

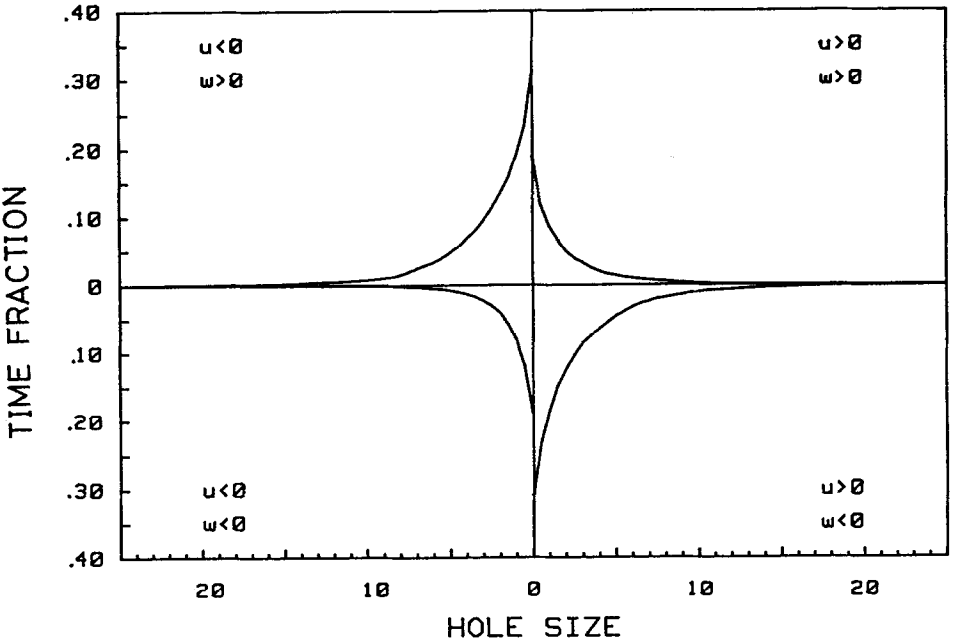

Fig. 5. Quadrant representation of time fraction of vertical momentum transport contribution, $T_{i,H}$.

The conditionally averaged momentum flux defined by (3) for the quadrant, i, is normalized by the mean flux as follows,

$$S_{i,H} = \langle uw \rangle_{i,H} / |\overline{uw}| \,. \tag{4}$$

And the fractional time interval $T_{i,H}$ in which $I_{i,H}(u(t), w(t)) = 1$ can be written as follows,

$$T_{i,H} = \lim_{T \to \infty} 1/T \int_0^{\infty} I_{i,H}(u(t), u(t))\, \mathrm{d}t \,. \tag{5}$$

Examples of the variation of $T_{i,H}$ and of the absolute value of $S_{i,H}$ with hole size, H, for each quadrant are shown in Figures 5 and 6, respectively, for Run 1. The values at $H = 0$ of $S_{i,H}$ in Figure 6 indicate the contribution to the total vertical momentum flux $-\overline{uw}$ from each quadrant. The values of $S_{i,H}$ for $i = 2$ and 4 are nearly the same at $H = 0$: 78 and 77%, respectively. They are much larger than those from $i = 1$ and 3, which are 30 and 25%. When $H \geqq 5$, $S_{i,H}$ for $i = 4$ is larger than that for $i = 2$. For example, the percentages of $S_{i,H}$ at $H = 10$ are 10% for $i = 2$ and 14% for $i = 4$, but values for $i = 1$ and 3 are very small only 2 and 0.3%, respectively. The values of $T_{i,H}$ for $H = 10$ are 0.2, 0.7, 0.03 and 1.0% for $i = 1$, 2, 3 and 4, respectively. This means that 24% of the total downward momentum flux is transported in only 1.7% of the total duration of the hole size when $H =$ 10. The intermittent structure of the downward transport of momentum can be appreciated from these results.

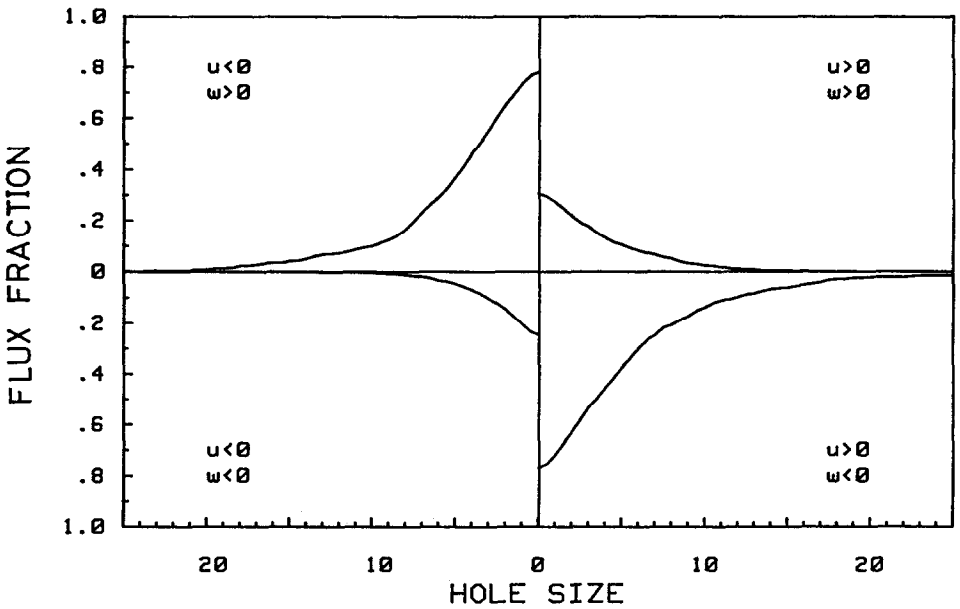

Fig. 6. Quadrant representation of the contribution for total vertical momentum flux, $S_{i,H}$.

5. Downward Momentum Transport During Extreme Wind Velocities

It is clear that the downward momentum flux is concentrated into intervals of short duration. To see the relation between downward momentum transport and the gust, conditional sampling was undertaken under the condition that the maximum of u must be larger than $3\sigma_u$. The averaged shape of the conditionally sampled traces of wind velocity u, w and vertical momentum transport uw are shown in Figure 7, which has been adjusted to the time of the maximum u value. Eleven events are detected for Run 1. As is clear in this figure, when u is at a maximum, w shows a negative value and uw forms a peak of downward transport at the same time. The conditionally averaged momentum flux $-\overline{uw}_c$ for 1 sec, from -0.5 to 0.5 sec around the peak gust, is evaluated to be $-8.96\ \mathrm{m^2\ s^{-2}}$, which is 4.17 times larger than the mean value of $-2.15\ \mathrm{m^2\ s^{-2}}$ for 30 min. Although the time fraction of the summation of the downward momentum flux for 1 sec of these events is only 0.61% of the whole observation duration of 30 min, the contribution of the momentum transport in the peak gust amounts to 2.55% of the total momentum transport in 30 min. The results of the other runs are tabulated in Table III.

The numbers of detected events are variable. The downward momentum flux for 1 sec at peak gust, $-\overline{uw}_c$ is as large as 5.53 times the mean momentum flux for a 30 min averaged average. The average contributions of downward momentum transport for 1 sec are 3.63% of the total momentum transport flux for 30 min,

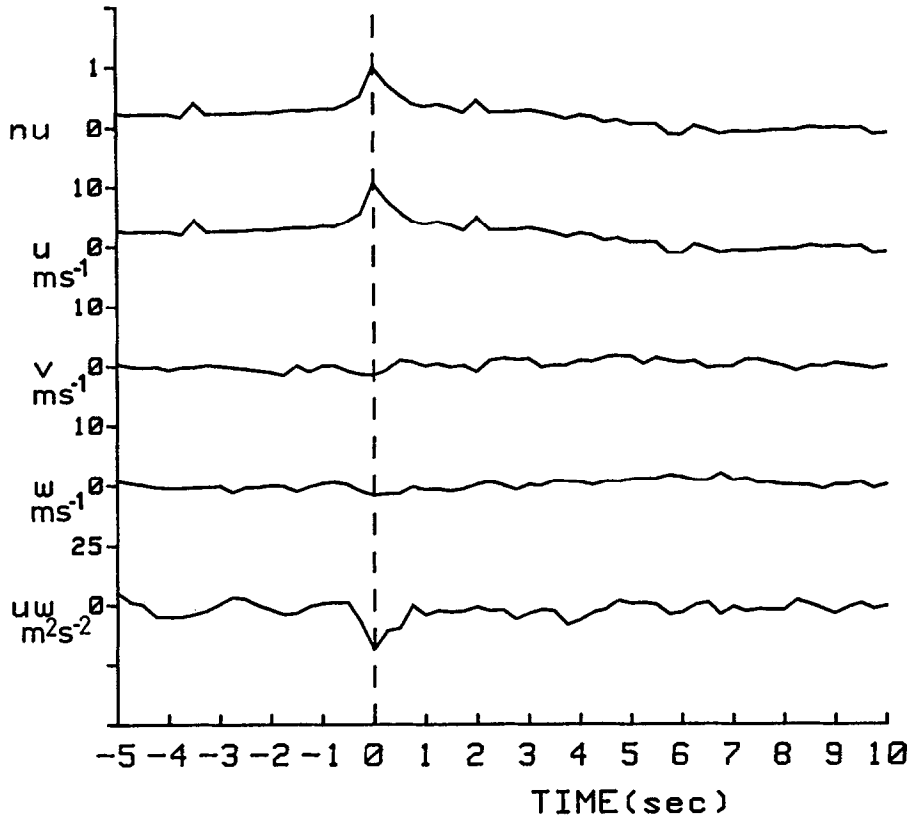

Fig. 7. Conditionally averaged wind velocity fluctuations of longitudinal and vertical components, u and w, and vertical momentum transport uw for 15 sec at the time of the peak gust; nu means the longitudinal wind velocity fluctuation by the value of the peak gust.

while the average time fraction is only 0.66% of the total time. The rate of transport of momentum is very efficient in the case of gusts.

The vertical transport of momentum has also been sampled when u was a minimum, with the condition that u be smaller than $-3\sigma_u$. As shown in Table IV, the detected events for 6 runs are only one or two except for Runs 8 and 9, when 6 and 4 events were found. This imbalance has already been shown in Section 4 and the contribution from $i = 2$ (ejection) is small compared to $i = 4$ (sweep).

6. Gust Front

Sherlock (1952) thought of a gust near the surface as part of a gust front coming down from higher levels as a front with high momentum. The intermittent nature of the vertical transport of momentum was first recognized by Mitsuta (1967) through field observations using a sonic anemometer near the ground. The phe-

TABLE III

The vertical momentum flux $-\overline{uw}_c$ for 1 sec conditionally sampled at peak gust(sweep), and the fraction to the total observation duration and the contribution to the total vertical transport of momentum, $-\overline{uw}$

Run	Detected event number	Total average flux $-\overline{uw}$ $m^2 s^{-2}$	Conditional average flux $-\overline{uw}_c$ $m^2 s^{-2}$	Ratio $-\overline{uw}_c/(-\overline{uw})$	Time fraction %	Transport contribution %
1	11	2.15	8.96	4.17	0.61	2.55
2	11	2.32	13.92	6.00	0.61	3.67
3	10	1.75	10.03	5.73	0.56	3.08
4	25	2.26	11.85	5.24	1.39	7.28
5	15	1.41	5.54	3.93	0.83	3.27
6	16	0.95	6.18	6.50	0.89	5.78
7	8	1.03	6.31	6.12	0.44	2.72
8	4	1.20	6.31	5.26	0.22	1.17
9	3	1.39	3.21	2.31	0.17	0.39
10	12	2.23	11.78	5.28	0.67	3.52
11	22	0.98	9.95	10.15	1.22	12.41
12	5	0.86	8.19	9.52	0.28	2.64
Mean	11.8	1.54	8.52	5.53	0.66	3.63
RMS	6.5	0.54	3.00		0.36	

TABLE IV

Same as Table III except for a lull (ejection)

Run	Detected event number	Total average flux $-\overline{uw}$ $m^2 s^{-2}$	Conditional average flux $-\overline{uw}_c$ $m^2 s^{-2}$	Ratio $-\overline{uw}_c/(-\overline{uw})$	Time fraction %	Transport contribution %
1	–	2.15	–	–	–	–
2	–	2.32	–	–	–	–
3	1	1.75	16.19	9.25	0.06	0.51
4	–	2.26	–	–	–	–
5	–	–	–	–	–	–
6	1	0.95	16.67	17.55	0.06	0.98
7	–	–	–	–	–	–
8	6	1.20	9.01	7.51	0.33	2.50
9	4	1.39	6.64	4.78	0.22	1.06
10	–	2.23	–	–	–	–
11	–	0.98	–	–	–	–
12	2	0.86	5.95	6.92	0.11	0.77

nomenon can also be detected in the statistical analysis of gusts in the previous section, viz., the $i = 4$ (sweep) is effective in vertical momentum transport. The structure of the gust front on the horizontal plane at 8.25 m height can be visualized in the spatial distribution of wind speed of the present anemometer network

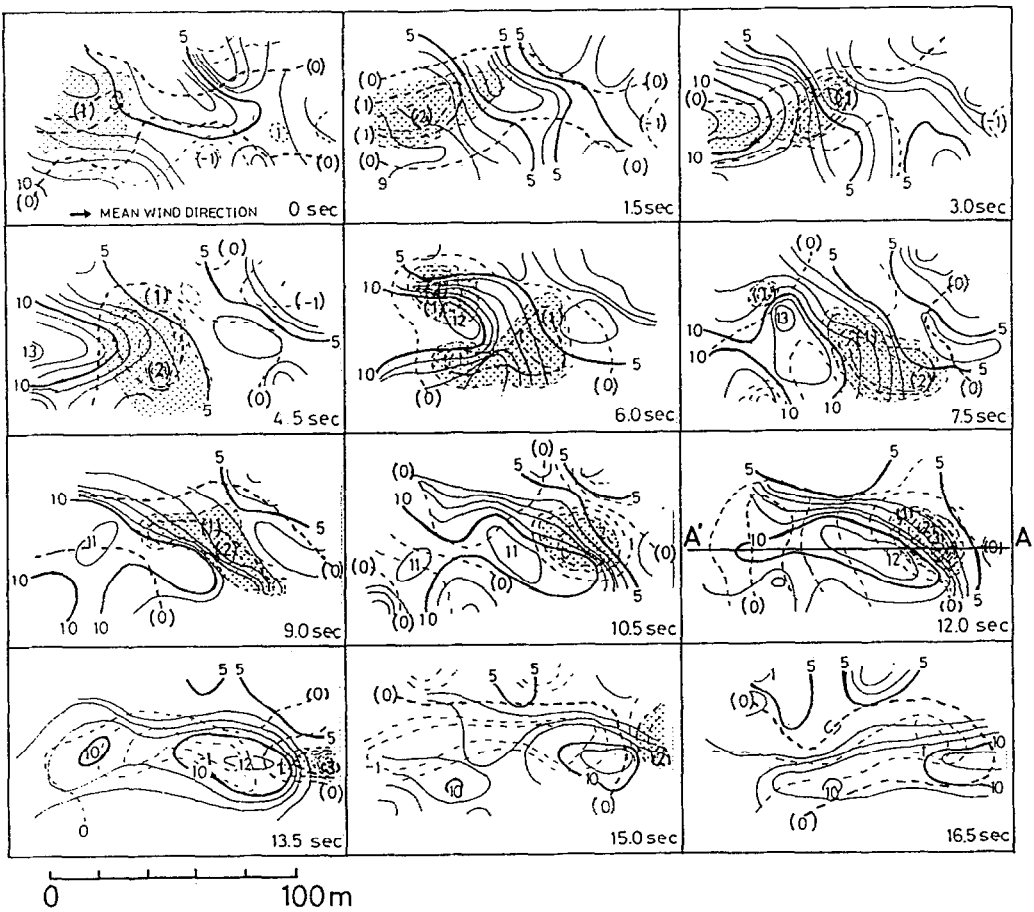

Fig. 8. Time series of horizontal distribution of wind speed and time derivative of wind speed. Isopleths are drawn every 1 m s^{-1} for wind speed and 0.5 m s^{-2} for time derivative. The shadowed area is where the value of the time derivative of wind speed is more than 0.5 m s^{-2}.

(Figure 1). An example (Run 6) of the time series of the horizontal distribution of wind speed for 1.5 sec intervals is shown in Figure 8. The distribution of the time derivative of wind speed is also shown in this figure. The averaging time of 1.5 sec for the wind speed is limited by the dynamic response of the cup anemometer (Hayashi, 1987). The isopleths are drawn every 1 m s^{-1} for wind speed and 0.5 m s^{-2} for the time derivative of wind speed.

The shadowed area is where the value of the time derivative of wind speed is positive and greater than 0.5 m s^{-2}. The high wind speed region (above 10 m s^{-1}, i.e., the gust front) appears in the upwind direction at 3.0 sec. This high speed region is more than 100 m long in the direction of the wind and 30 m wide at 12.0 sec. The isotachs are crowded at the front of this high wind region and sparse to its rear. This illustrates very well the horizontal structure of the gust front. In the high wind area following the gust front, the horizontal gradient is not so large

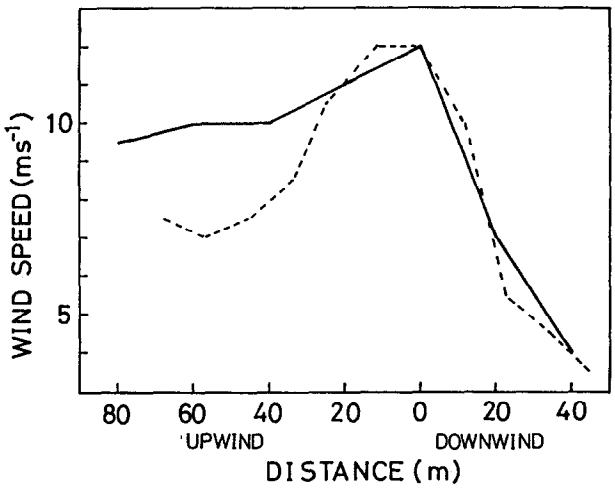

Fig. 9. The cross-section of wind speed along the wind direction of $A - A'$ in Figure 8. The dashed line shows the estimated horizontal distribution of the gust front calculated from the time change of wind speed at one point by replacing the distance with the product of the moving speed of the gust front and the time lag.

and the wind speed begins to decrease gradually. The wind speed distribution along the line ($A - A'$) crossing the gust front at 12.0 sec is shown in Figure 9. The spatial wind speed gradient shown in this figure is $2.0 \cdot 10^{-1}\,s^{-1}$ in the front part and $1.9 \cdot 10^{-2}\,s^{-1}$ to the rear. One anemometer reveals a sudden increase and then a slow decrease of wind speed at the passage of the high wind area. The maximum of time change of wind speed reaches $3.5\,m\,s^{-2}$ in front of the high wind speed section at 12.0 sec.

As the gust front moves, it varies its shape. Therefore the instantaneous moving speed of the gust front is hard to determine. The mean moving speed can be defined using the distance and the time of the passage of the gust front across the anemometer network. The mean motion is estimated as $7.5\,m\,s^{-1}$, which is the same as the ensemble mean of wind speed of $7.5\,m\,s^{-1}$ of the 28 anemometers for 12 sec. The estimated horizontal distribution of wind speeds is also shown in Figure 9, calculated from the time change of wind speed observed at one point (No. 22 in Figure 1) by replacing distance by the product of the moving speed of the gust front and the time lag. Both wind distributions coincide well at the frontal peak, but to the rear, the estimated wind speed is smaller than the observed one. This means that the air following the gust front moves slower than the gust front and the high wind area stretches leeward.

7. The Gust Front and Downward Momentum Transport

The gust front is the moving area of sudden increase in wind speed. The development of the front cannot be recognized from Eulerian information such as the

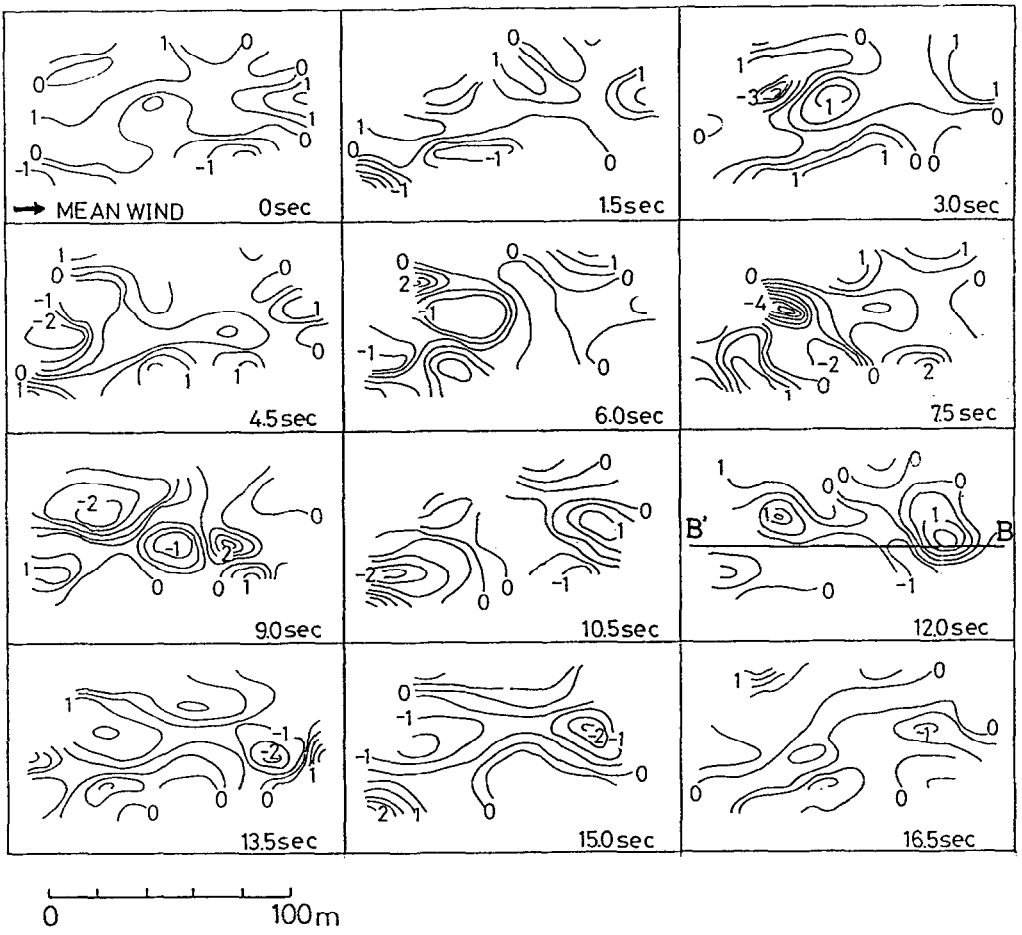

Fig. 10. Time series of the horizontal distribution of Langrangian acceleration calculated from the wind speed data of Figure 8. Isopleths are drawn every 0.5 m s^{-2}.

spatial distribution of wind speed or its time derivative as a function of location. With a Langrangian treatment, however, these problems disappear. The acceleration or deceleration of the gust front is closely related to its development. The Langrangian derivative of the windward velocity can be written as follows, neglecting lateral and vertical motions,

$$DU/Dt = \partial U/\partial t + U\partial U/\partial x\,, \tag{6}$$

where U is wind velocity. Two terms on the right-hand side, $\partial U/\partial t$ and $U\partial U/\partial x$, can be calculated from the time and space distribution of wind speed by replacing the windward velocity with the wind speed. An example of a time series of the distribution of the Langrangian derivative of wind speed DU/Dt is shown in Figure 10. DU/Dt is calculated using the same time series of the spatial distribution of wind speed as in Figure 8. The region of positive DU/Dt moves from 9.0 to

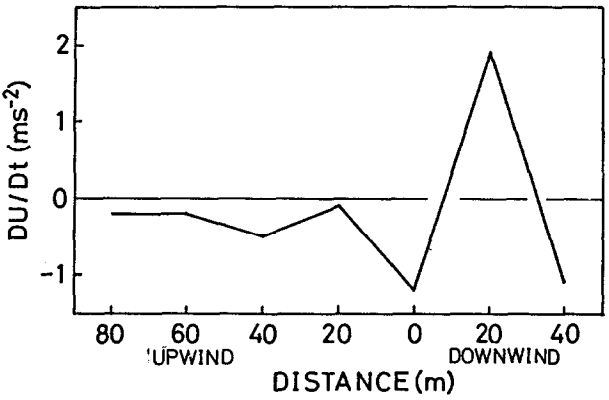

Fig. 11. The cross-section of the Langrangian acceleration along the wind direction $B - B'$ in Figure 10.

12.0 sec in the anemometer network and their region corresponds to the gust front in Figure 8. The acceleration of the gust front means that the gust front is still developing. The distribution of DU/Dt along the windward line ($B - B'$) is shown in Figure 11. The origin is at the peak wind speed as in Figure 9. The value of DU/Dt is positive, corresponding to the forward edge of the gust front with a maximum at about 20 m from the origin and is negative to the rear of the high wind region. This corresponds to an accelerating gust front.

The equation of motion for the mean flow in the windward direction in the atmospheric surface layer is expressed as follows,

$$DU/Dt = -1/\rho \cdot \partial P/\partial x + \partial(-\overline{uw})/\partial z + \nu \cdot \partial(\partial U)/\partial x_i \, \partial x_i \,, \tag{7}$$

where U is the mean wind velocity, ρ the air density, P the atmospheric static pressure and ν the molecular viscosity. The horizontal momentum flux is neglected. If the pressure gradient term and the molecular viscous term are neglected, Equation (7) can be written as,

$$DU/Dt = \partial(-\overline{uw})/\partial z \,. \tag{8}$$

The gust front seems to be accelerating as a result of convergence of the downward momentum flux. In applying Equation (8) to the gust front, U is the wind speed averaged over a 1.5 sec interval (cup anemometer measurements) and $-\overline{uw}$ is the downward momentum flux averaged over the same time period. The divergence of downward momentum transport is calculated in the layer between heights of 8.25 and 12 m. The downward momentum transport at a height of 12 m is calculated from the two components of wind fluctuation u and w directly measured by the sonic anemometer and the bulk method is used at the lower height of 8.25 m as the intermittent motion decreases with decreasing height. Then, the following equation can be written.

$$\partial(-uw)/\partial z = (-\overline{uw} - C_d \cdot U^2)/\Delta z \,. \tag{9}$$

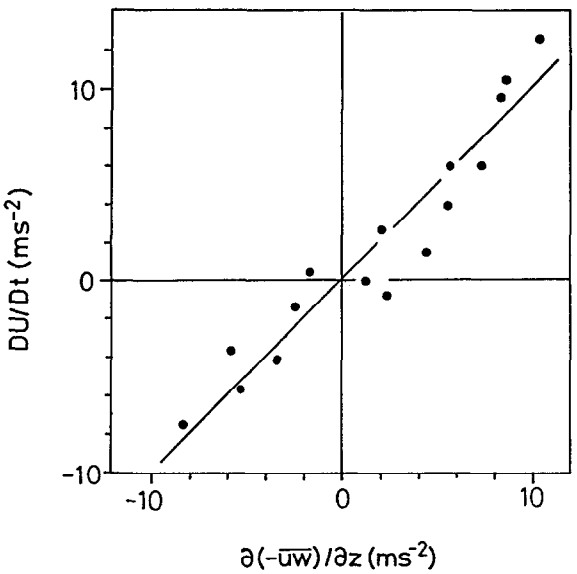

Fig. 12. The relation of the vertical gradient of downward momentum flux for 1.5 sec and the Lagrangian acceleration of the gust front. The straight line shows the regression with a slope of 1.0.

where C_d is the drag coefficient and Δz is the difference in height. The drag coefficient C_d at a height of 8.25 m is estimated from the value at a height of 12 m. Since the vertical momentum flux in neutral conditions and the mean wind profile obey the same log law, the momentum flux $-\overline{uw}$ is expressed using the mean wind speed U_1 and U_2 at levels z_1 and z_2 as follows,

$$-\overline{uw} = u_*^2 = C_{d1}U_1^2 = C_{d2}U_2^2, \tag{10}$$

where u_* is the friction velocity, and C_{d1} and C_{d2} are the drag coefficients at levels z_1 and z_2. The C_{d1} is calculated from C_{d2} using the log profile of wind speed and Equation (10) as follows,

$$C_{d2} = (C_{d2}^{-1/2} - k^{-1} \cdot \log(z_1/z_2))^{-2}, \tag{11}$$

where k is the kármán constant (0.4). The drag coefficient C_{d2} at a height of 8.25 m is calculated as $1.70 \cdot 10^{-2}$ from the observed value of $C_{d1} = 1.35 \cdot 10^{-2}$ at a height of 12 m, which is obtained from the mean wind velocity and momentum flux in Tables I and II.

The relation between the gradient of the downward momentum transport $\partial(-\overline{uw})/\partial z$ and the Lagrangian acceleration of the gust front DU/Dt is shown in Figure 12 for 16 samples. DU/Dt and $\partial(-\overline{uw})/\partial z$ are clearly correlated positively. The slope of the regression line is 1.0 as expected from Equation (8). The convergence of the downward momentum transport maintains the acceleration of the gust front.

8. Conclusions

The probability density of wind velocity components deviates from a Gaussian distribution for values far from their mean values. More than several times the mean downward momentum are transported almost instantaneously by the sweep and ejection phenomena. The sweep phenomena make a primary contribution to the large transport of downward momentum. The downward momentum transport in a peak gust is very efficient, 3.63% of total downward momentum being transported in only 0.66% of the total time.

The high wind region consists of a sudden increase of wind speed at the front and a slow decrease to its rear. The high wind region stretches leeward for more than 100 m and its width is about 30 m. The gust front can be seen at the forward edge of the high wind region. The time derivative of wind speed reaches a maximum of 3.5 $m\,s^{-2}$ ahead of the gust front.

The Langrangian treatment shows that the acceleration of a gust front balances the vertical convergence of downward turbulent momentum transport. This means that the development of the gust front is maintained by the convergence of downward momentum.

Acknowledgments

The author expresses his thanks to Prof. Y. Mitsuta of the Disaster Prevention Research Institute, Kyoto University for his useful discussions and critical comments throughout the study. Thanks are also due to Mr. T. Ozaki and Mr. S. Kawauchi for their assistance in the field observations.

References

Antonia, R. A., Chambers, A. J., Friehe, C. A., and Van Atta, C. W.: 1979, 'Temperature Ramps in the Atmospheric Surface Layer', *J. Atmos. Sci.* **36**, 99–108.

Blackwelder, R. F. and Kaplan, R. E.: 1976, 'On the Wall Structure of the Turbulent Boundary Layer', *J. Fluid Mech.* **76**, 89–112.

Chen, C. P. and Blackwelder, R. F.: 1978, 'Large-scale Motion in a Turbulent Boundary Layer: a Study Using Temperature Contaminations', *J. Fluid Mech.* **89**, 1–31.

Finnigan, J. J.: 1979, 'Turbulence in Waving Wheat. II: Structure of Momentum Transfer', *Boundary-Layer Meteorol.* **16**, 213–236.

Gao, W., Shaw, R. H., and Paw, U, K. T.: 1989, 'Observation of Organized Structure in Turbulent Flow within and Above a Forest Canopy', *Boundary-Layer Meteorol.* **47**, 349–377.

Grass, A. J.: 1971, 'Structural Features of Turbulent Flow over Smooth and Rough Boundaries', *J. Fluid Mech.* **50**, 233–256.

Hayashi, T.: 1987, 'Dynamic Response of a Cup Anemometer', *J. Atmos. Oceanic Tech.* **2**, 281–287.

Hayashi, T.: 1991, 'The Horizontal Distribution of Space Correlation Coefficients of Wind Fluctuations in the Atmospheric Surface Layer', *Boundary-Layer Meteorol.* **55**, 125–140.

Inoue, E.: 1955, 'Studies of the Phenomena of Waving Plants (Honami) Caused by Winds. Part 1: Mechanism and Characteristics of Waving Plants Phenomena', *J. Agric. Meteorol.* (Japan) **11**, 18–22.

Kline, S. J., Reynolds, W. C., Shraub, F. A., and Rundstadler, P. W.: 1967, 'The Structure of Turbulent Boundary Layer's, *J. Fluid Mech.* **30**, 741–773.

Lu, S. S. and Willmarth, W. W.: 1973, 'Measurement of the Structure of the Reynolds Stress in a Turbulent Boundary Layer', *J. Fluid Mech.* **60**, 481–511.

Mitsuta, Y.: 1967, 'Some Results of Direct Measurements of Momentum Flux in the Atmospheric Boundary Layer by Sonic Anemometer', *J. Meteorol. Soc.*, Japan **46**, 29–35.

Mitsuta, Y.: 1974, 'Sonic Anemometer-Thermometer for Atmospheric Turbulence Measurements, Flow: its Measurement and Control in Science and Industry', R. B. Dowell (ed.), *Instrument Society of America*, Vol. 1, pp. 341–348.

Nakagawa, H. and Nezu, I.: 1977, 'Prediction of the Contribution to the Reynolds Stress from Bursting Events in Open-Channel Flows', *J. Fluid Mech.* **80**, 99–128.

Raupach, M. R.: 1981, 'Statistics of Reynolds Stress in Rough-wall and Smooth-wall Turbulent Boundary Layers', *J. Fluid Mech.* **108**, 363–382.

Shaw, R. H., Tavanger, J., and Ward, D. P.: 1983, 'Structure of the Reynolds Stress in a Canopy Layer', *J. Climate Appl. Meteorol.* **22**, 1922–1931.

Schols, J. L. J.: 1984, 'The Detection and Measurement of Turbulent Structure in the Atmospheric Surface Layer', *Boundary-Layer Meteorol.* **29**, 39–58.

Wallace, J. M., Eckelmann, H., and Brodky, R. S.: 1972, 'The Wall Region in Turbulent Shear Flow', *J. Fluid Mech.* **54**, 39–48.

Willmarth, W. W. and Lu, S. S.: 1972, 'Structure of the Reynolds Stress near the Wall', *J. Fluid Mech.* **55**, 65–92.